Supplementary Information

Transparent-Conductive-Oxide-Free Front Contacts for High Efficiency Silicon Heterojunction Solar Cells

Shenghao Li[1,2], Manuel Pomaska[1], Andreas Lambertz[1], Weiyuan Duan[1], Karsten Bittkau[1], Depeng Qiu[1,3], Zhirong Yao[1,2], Martina Luysberg[4], Paul Steuter[1,3], Malte Köhler[1,3], Kaifu Qiu[1,2], Ruijiang Hong[2], Hui Shen[2,5], Friedhelm Finger[1], Thomas Kirchartz[1,6], Uwe Rau[1,3] and Kaining Ding[1]

[1]IEK-5 Photovoltaik, Forschungszentrum Jülich, 52425 Jülich, Germany

[2]Institute for Solar Energy Systems, Guangdong Provincial Key Laboratory of Photovoltaic Technology, School of Physics, Sun Yat-Sen University, 510006 Guangzhou, China

[3]Faculty of Electrical Engineering and Information Technology, RWTH Aachen University, Mies-van-der-Rohe-Straße 15, 52074 Aachen, Germany

[4]Ernst Ruska-Centre for Microscopy and Spectroscopy with Electrons, Forschungszentrum Jülich, 52425 Jülich, Germany

[5]Jiangsu Collaborative Innovation Center of Photovoltaic Science and Engineering, Changzhou University, 213164 Changzhou, China

[6]Faculty of Engineering and CENIDE, University of Duisburg-Essen, Carl-Benz-Str. 199, 47057 Duisburg, Germany

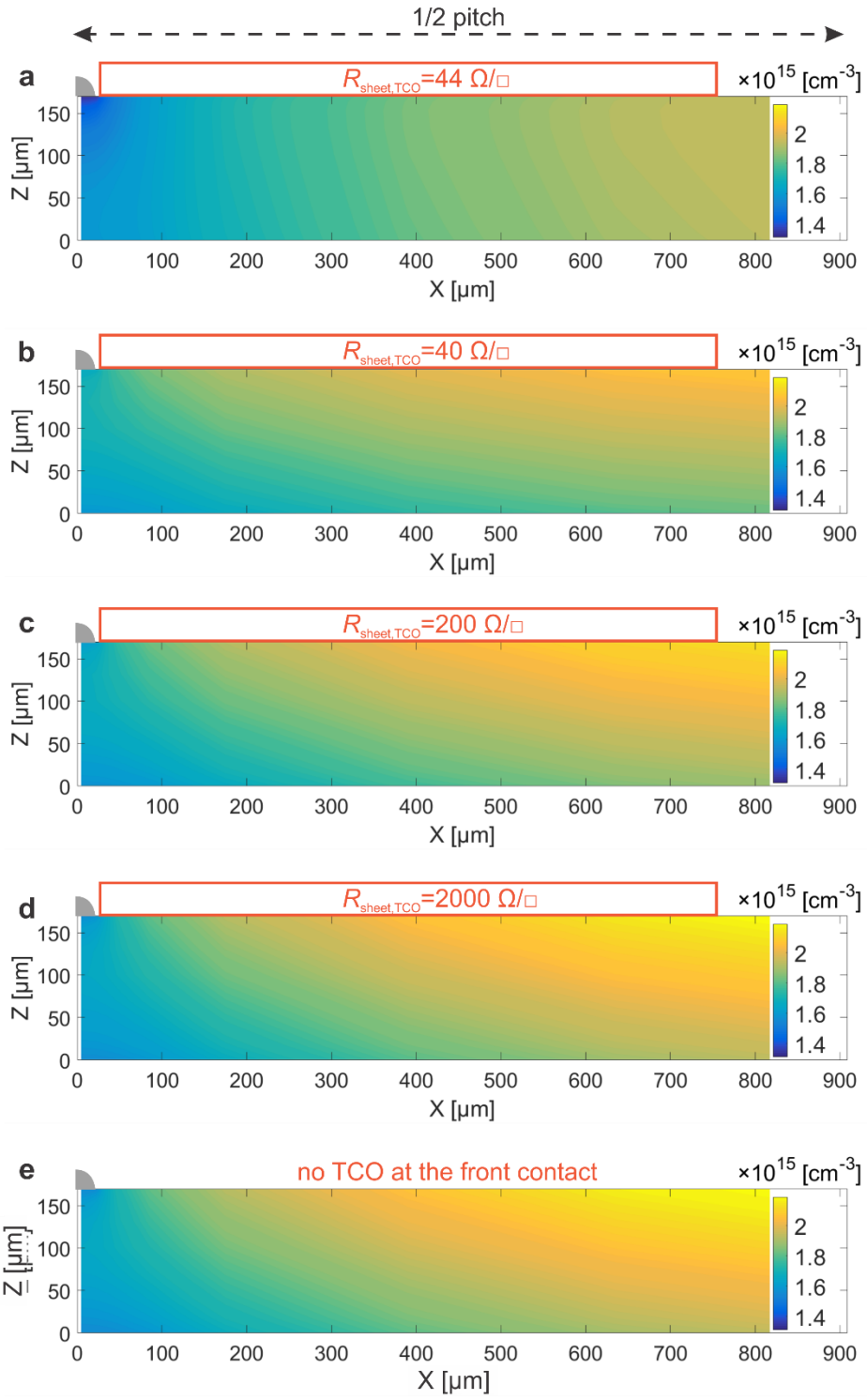

FIG. S1 | Simulated cross-section images of excess carrier distribution in the c-Si bulk of SHJ solar cells. **a,** Front junction SHJ solar cell with front TCO sheet resistance of 44 Ω/□, **c-d,** Rear junction SHJ solar cells with different front-side TCO layers. **e,** Rear junction solar cells without front-side TCO for carrier collection.

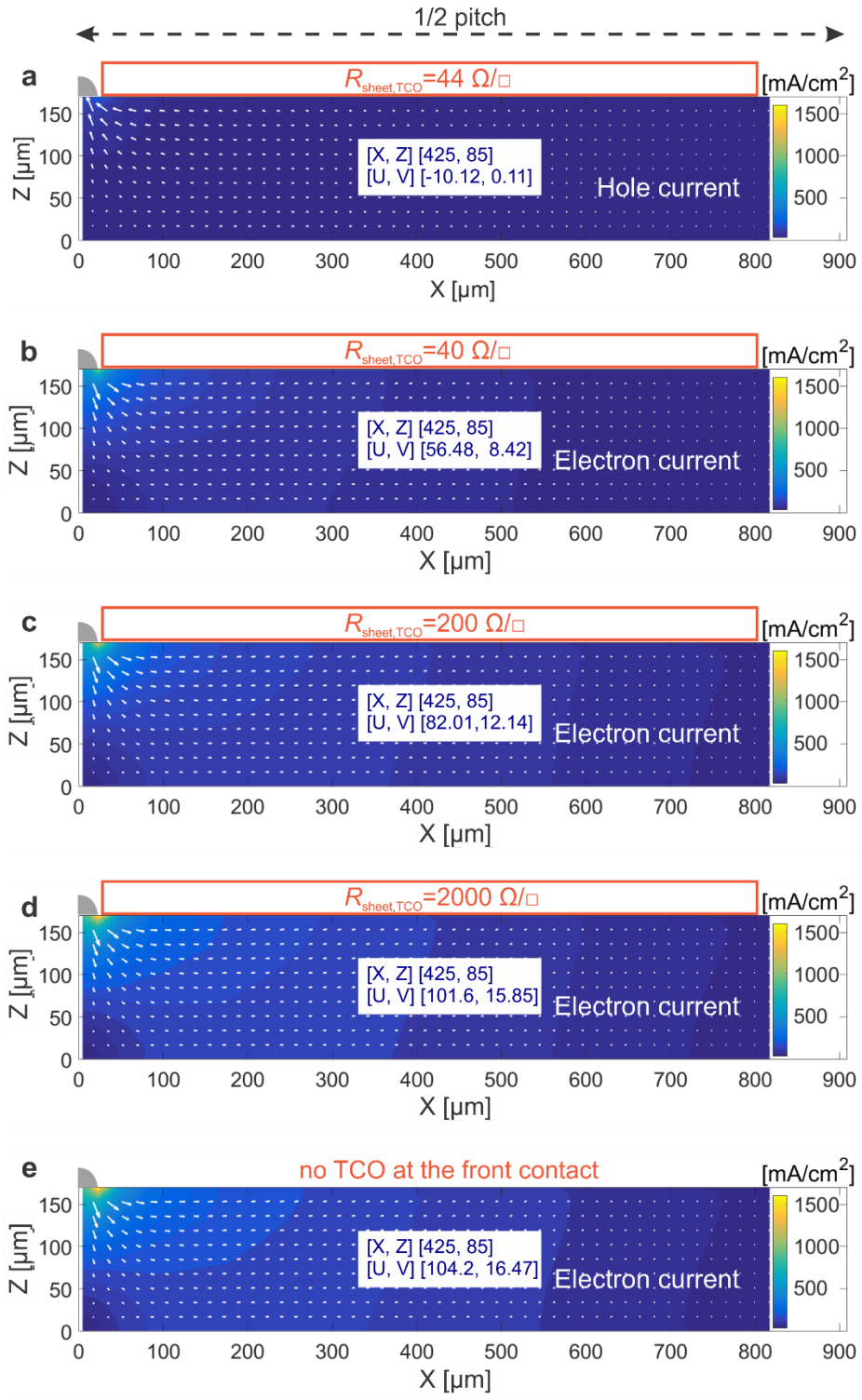

FIG. S2 | Simulated cross-section images of current density distribution in the c-Si bulk of SHJ solar cells. **a,** Front junction SHJ solar cell with front TCO sheet resistance of 44 Ω/□, **c-d,** Rear junction SHJ solar cells with different front-side TCO layers. **e,** Rear junction solar cells without front-side TCO for carrier collection. The text boxes in the middle show the vector of current flows [U, V] in the position [X, Y].

Fig. S1 shows the simulated excess carrier distribution in the c-Si bulk under 1 sun illumination. The excess carrier density is below 2.2×10^{15} cm^{-3}, which is about half of the doping concentration of the c-Si bulk (4.5×10^{15} cm^{-3}). The excess carrier density is lower in front junction than in rear junction solar cells. As the TCO sheet resistance reduces, the excess carrier density increases in the c-Si bulk. The lateral gradience in excess carrier distribution indicates a diffused current in the bulk.

Fig. S2 shows the simulated carrier current distribution inside the c-Si bulk. The result shows that for both front junction and rear junction SHJ solar cells, the bulk conduction contributes to the carrier collection. As shown in Fig. S2a and S2b, there are lateral electron currents in the c-Si bulk even when the sheet resistance (R_{sheet}) of TCO is quite low. On the other hand, the current density is much higher in rear junction SHJ solar cell than in front junction SHJ solar cell with similar TCO sheet resistance. As the TCO sheet resistance increases from 40 Ω/□ to 2000 Ω/□ in rear junction solar cells, the electron currents in the c-Si bulk increases as shown in Fig. S1b-S1d, which indicates that the currents in the TCO layers transfer to the bulk with decreasing TCO lateral conduction. When the TCO is completely removed (Fig. S2e), all the currents are transferred to the c-Si bulk and the c-Si bulk takes over the whole lateral conduction for the solar cell.

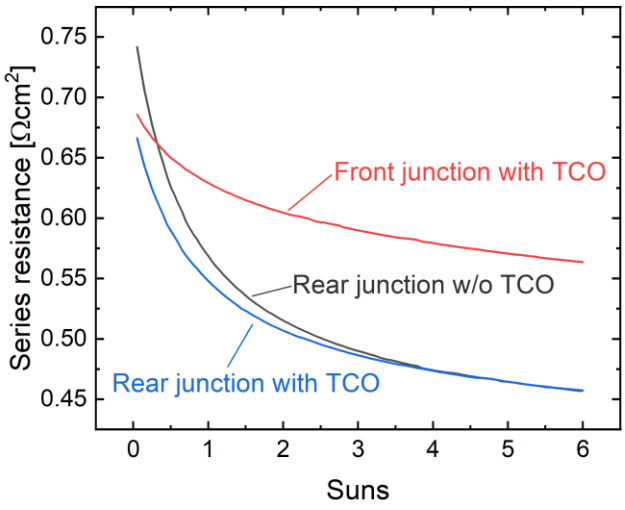

Figure S3 | Simulated series resistance versus illumination intensity for SHJ solar cells with different structures. For the simulation results, the TCO sheet resistance was set as 160 Ω/□ for both front junction and rear junction SHJ solar cells, respectively. The simulated series resistance was calculated from the integral of the resistive losses in the model.

It is worth noting in Fig. S3 that for rear junction solar cells, although the series resistance is slightly higher for TCO-free solar cell than with TCO at 1 sun, the series resistance becomes the same when the illumination increases to over 4 suns. This indicates that at high illuminations, the conduction in absorber dominates the lateral conduction, and the mild lateral collection advantage with front TCO has vanished.

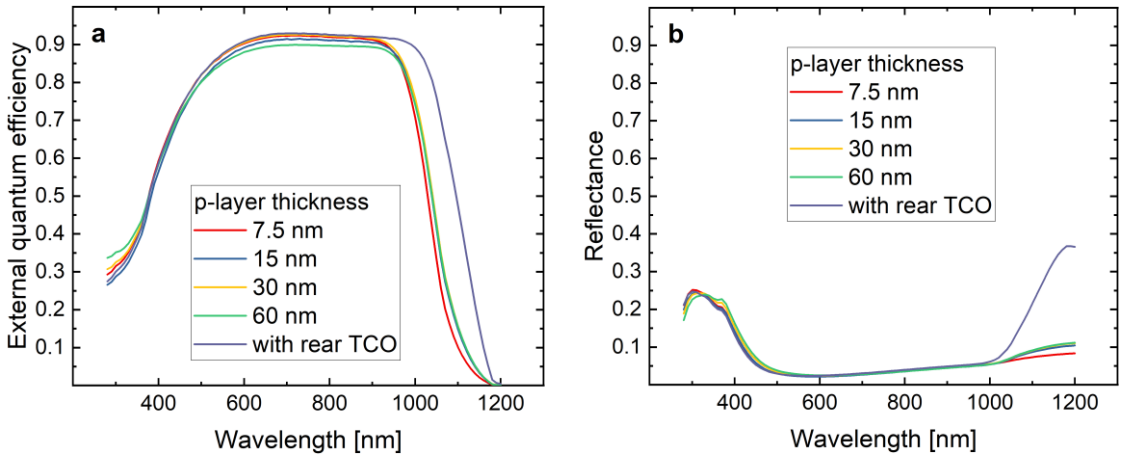

Figure S4 | Optical spectra comparing both side and front side TCO-free SHJ solar cells. a, External quantum efficiency spectra and **b,** Reflectance spectra.

With lateral c-Si bulk conduction, we are able to stop relying on TCO for the conduction. However, when the rear side TCO was removed, the short-circuit current density reduces. In Figure S4, the external quantum efficiency and reflectance are compared for the solar cells with and without rear TCO. Higher reflectance in long wavelength was observed when the solar cell uses rear side TCO, which gives rise to the higher external quantum efficiency absorption in the long wavelength range. It has been reported that Ti is a poor back reflector for solar cells[1]. A good back reflector is needed in the coming development to improve the optical absorption[2,3].

Although the parasitic absorption of TCO layer is removed in front-side TCO-free solar cells giving rise to 1 mA/cm^2 increase in external quantum efficiency, the short-circuit current density is not prominently improved. The reason is shown in Fig. S5a. Compared to conventional SHJ solar cell with front TCO, the external quantum efficiency drops more severe for the front TCO-free SHJ solar cell when the fingers is included in the measurement. Both samples are screen printed in a similar process with low temperature silver paste for SHJ solar cells, indicating similar finger widths (Ti/Au/Ag contact is fabricated before screen printing for TCO-free solar cells but

there is minor influence in the finger width). Electroluminescence (EL) was performed on front-side TCO-free SHJ solar cells with screen printed finger contact and thermal evaporated silver fingers, respectively, as shown in Fig. S5b. The EL signal shows a flat luminous intensity between fingers for the sample with evaporated fingers, while a round shape luminous intensity is shown when screen printed fingers is used. This could indicate a current loss in the area adjacent to the finger. The microscopy image of screen-printed finger in Fig. S5c reveals a spreading of organic solvent beside the finger. After printing the finger, organic solvent spreads out from the fingers before it is dry out in the annealing oven.

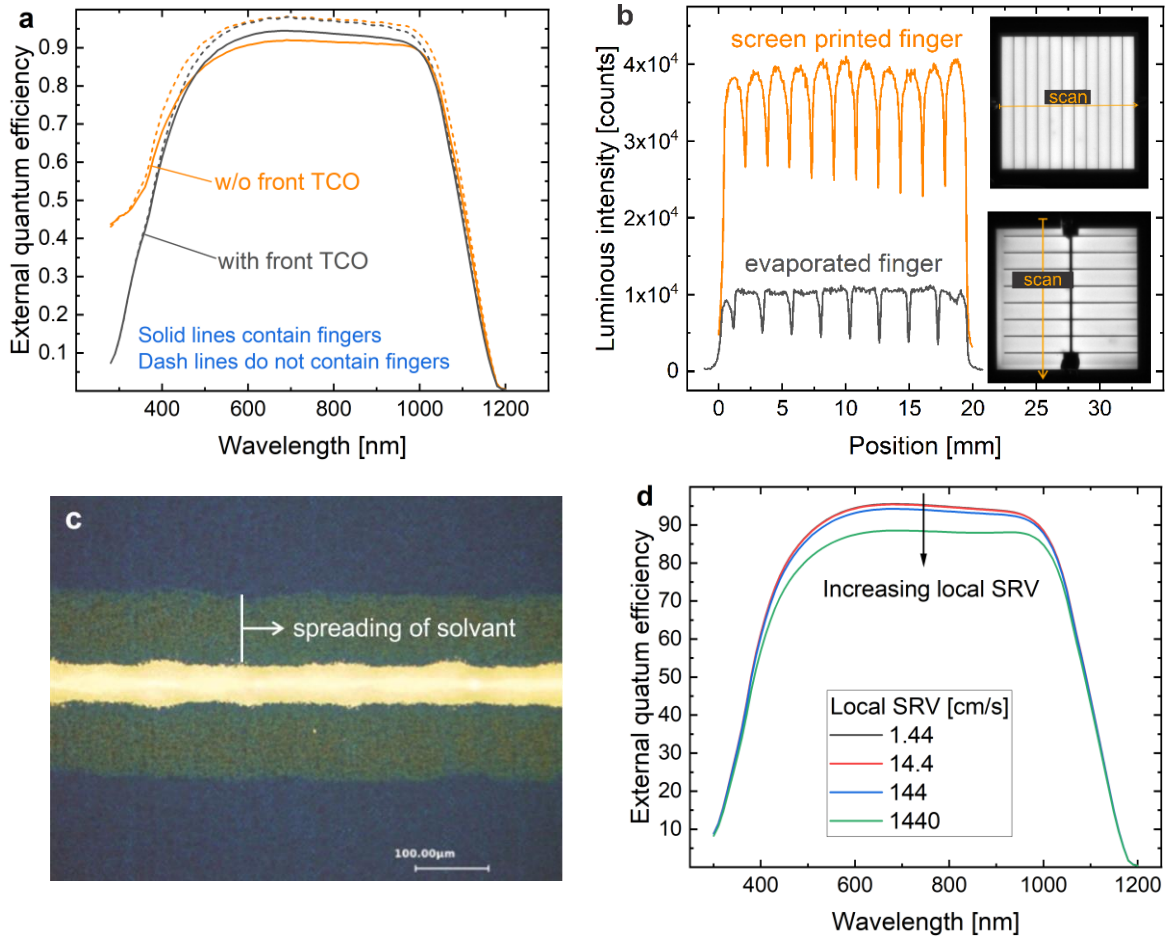

Figure S5 | Influence of metallization on front-side TCO-free SHJ solar cells. a, External quantum efficiency comparison between SHJ solar cells with and without front-side TCO layer. **b,** Electroluminescence comparison between screen printed finger and evaporated finger for front-side TCO-free solar cells. **c,** Optical microscopy image of a screen-printed finger. **d,** Simulated external quantum efficiency with different local surface recombination velocity around the finger area for front-side TCO-free solar cells.

Although the parasitic absorption of TCO layer is removed in front-side TCO-free solar cells giving rise to 1 mA/cm^2 increase in external quantum efficiency, the short-circuit current density is not prominently improved. The reason is shown in Fig. S5a. Compared to conventional SHJ solar cell with front TCO, the external quantum efficiency drops more severe for the front TCO-free SHJ solar cell when the fingers is included in the measurement. Both samples are screen printed in a similar process with low temperature silver paste for SHJ solar cells, indicating similar finger widths (Ti/Au/Ag contact is fabricated before screen printing for TCO-free solar cells but there is minor influence in the finger shading loss). Electroluminescence (EL) was performed on front side TCO-free SHJ solar cells with screen printed finger contact and thermal evaporated silver fingers, respectively, as shown in Fig. S5b. The EL signal shows a flat luminous intensity between fingers for the sample with evaporated fingers, while a round shape luminous intensity is shown when screen printed fingers is used. This could indicate a current loss in the area adjacent to the screen-printed fingers. The microscopy image of screen-printed finger in Fig. S5c reveals a spreading of organic solvent beside the finger. After printing the finger, organic solvent spreads out from the fingers before it is dry out in the annealing oven.

It is not clear yet how the organic solvent affects the external quantum efficiency and EL image. Simulation in Fig. S5d shows that the reduced local passivation adjacent to the finger area reduces the external quantum efficiency. However, an open-circuit voltage of over 730 mV was achieved for the front-side TCO-free SHJ solar cell, which indicates a decent passivation quality. On the other hand, influence could be in the optics, which is reflected in the different color in the area of organic solvent spreading as shown in Fig. S5c. Nevertheless, these results indicate that the current screen-printing silver paste for SHJ solar cell is not well adapted to this design with no TCO as buffer layer, and a suitable metallization method has to be developed before mass production of TCO-free SHJ solar cells.

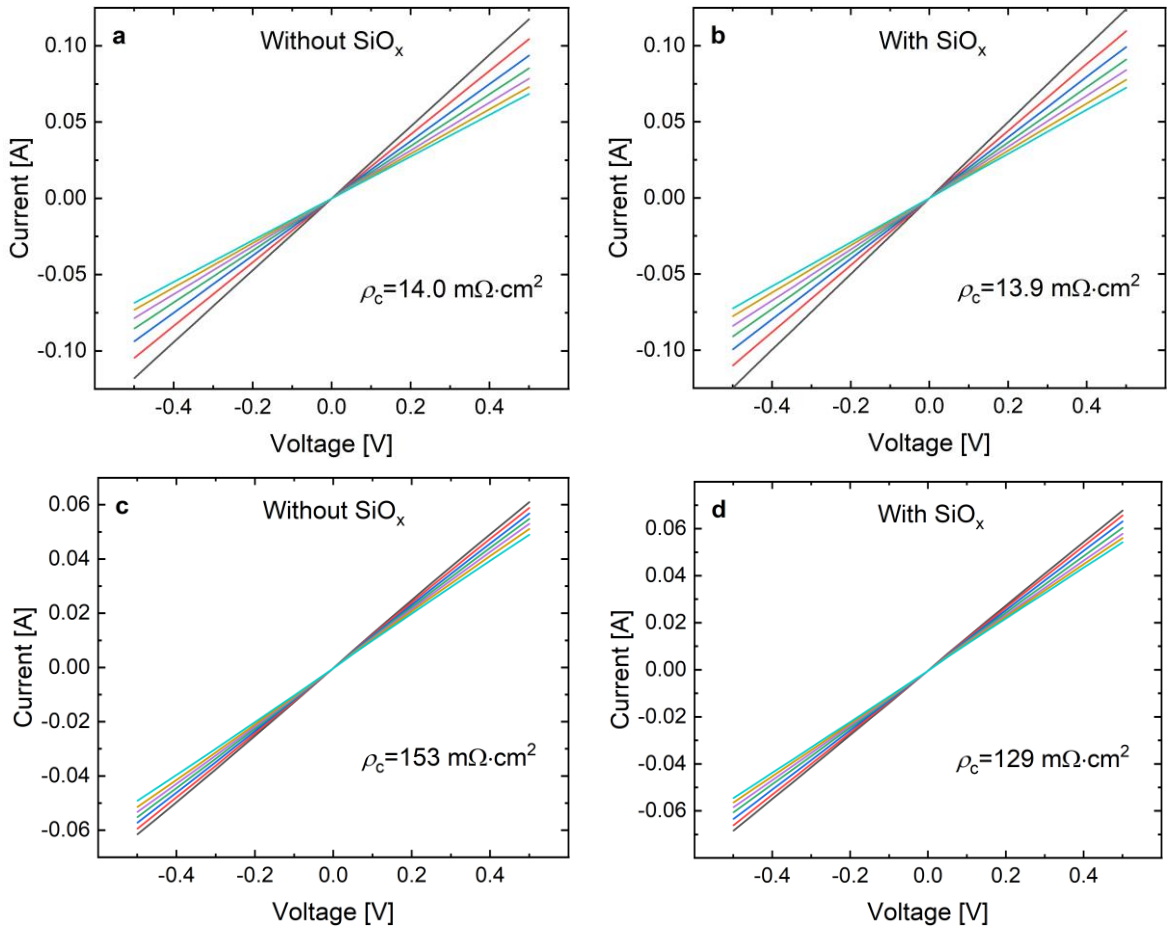

Figure S6 | TLM measurement on a-Si:H and Ti/Au/Ag contacts. 15 nm a-Si:H(n^+)/metal contacts **a,** without and **b,** with ozone oxidation treatment. And 30 nm a-Si:H(p^+) contacts/metal **c,** without and **d,** with ozone oxidation treatment.

The contact resistivities of a-Si:H and Ti/Au/Ag metal stacks are shown in Fig. S6. Before performing ozone oxidation on the interface, the contact resistivity of a-Si:H (p^+)/metal stack is about 10 times higher than that in a-Si:H (n^+)/metal stack. For both a-Si:H(p^+)/metal and a-Si:H(n^+)/metal contacts, the contact resistivity does not increase when an extra ozone oxidation process was introduced. The constant contact resistivity is explained by that titanium forms excellent contacts with silicon by reacting with the interface silicon oxide during evaporation process[4]. For the solar cell performance, the open-circuit voltage is improved while the fill factor is not influenced by the insert of the oxide layer.

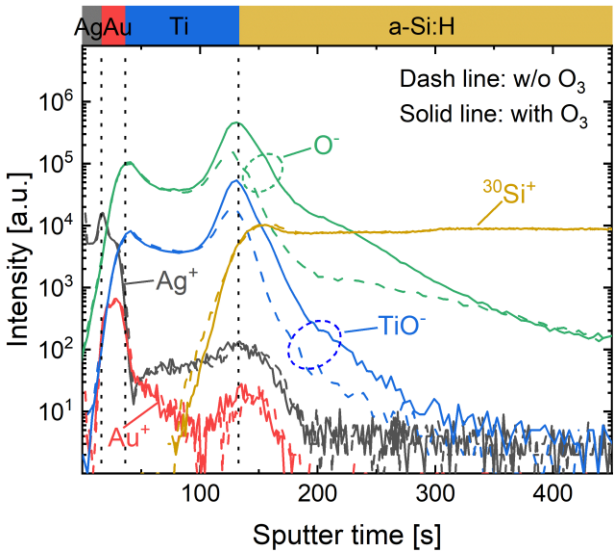

Figure S7 | Secondary ion mass spectrometry spectra at the metal and a-Si:H interfaces. The Ag^+, Au^+ and $^{30}Si^+$ spectra were measured with O_2 sputtering, while TiO^- and O^- spectra were measured with Cs sputtering. Due to the different sputter speed using O_2 and Cs, the spectra of TiO^- and O^- were expanded by 2.5 times.

The metal/a-Si:H interface was further explored by secondary ion mass spectrometry (SIMS), as shown in Fig S7. The SIMS measurement shows that the TiO^- and O^- signal increases at the Ti/a-Si:H interface with ozone oxidation, which proves that oxide layer is formed by ozone process. For the metal diffusion, it can be observed that Ag and Au diffuse into Ti layer. On the other hand, the metal diffusion into a-Si:H is not clearly shown due to the detection limit.

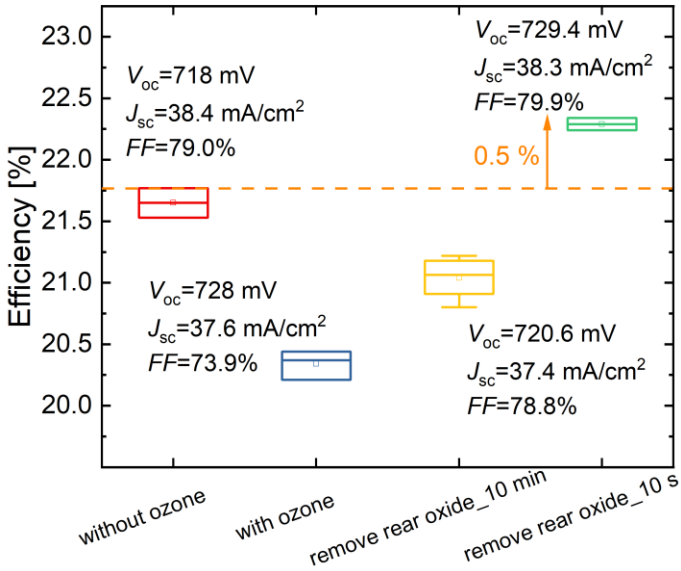

Figure S8 | Development of integrating ozone oxidation into TCO-free SHJ solar cell.

When the ozone oxidation was applied on the TCO-free SHJ solar cells, the open-circuit voltage was improved, showing a good protection effect for the a-Si:H/metal contacts. However, a low fill factor was measured even though the a-Si:H/metal contact resistivity is almost the same after ozone treatment. The low fill factor was then solved by HF etching of the SiO_x grown on the rear surface. This indicates that the low FF results from a poor rear contact of a-Si:H(p^+)/SiO_x/ITO. The HF rear etching time was then reduced from 10 min to 10 s to avoid the HF damage on passivation of the rear surface. By doing so, an efficiency improvement of $0.5\%_{abs}$ was achieved by integrating the ozone oxidation into the TCO-free SHJ solar cells. And a comparison in Table S1 indicates a superior performance of the TCO-free SHJ solar cell reported in this work.

Table S1 comparison of front-side TCO-free SHJ solar cells

	Front side metallization	Finger width [μm]	Pitch [mm]	*FF* [%]	V_{oc} [mV]	J_{sc} [mA/cm^2]	η [%]
Choi's work[5]	photolithography	2-3	0.2	75.3	608	37.1	17.0
In this work	Evaporation and screen printing	55-65	1.8	79.9	729.4	38.3	22.3

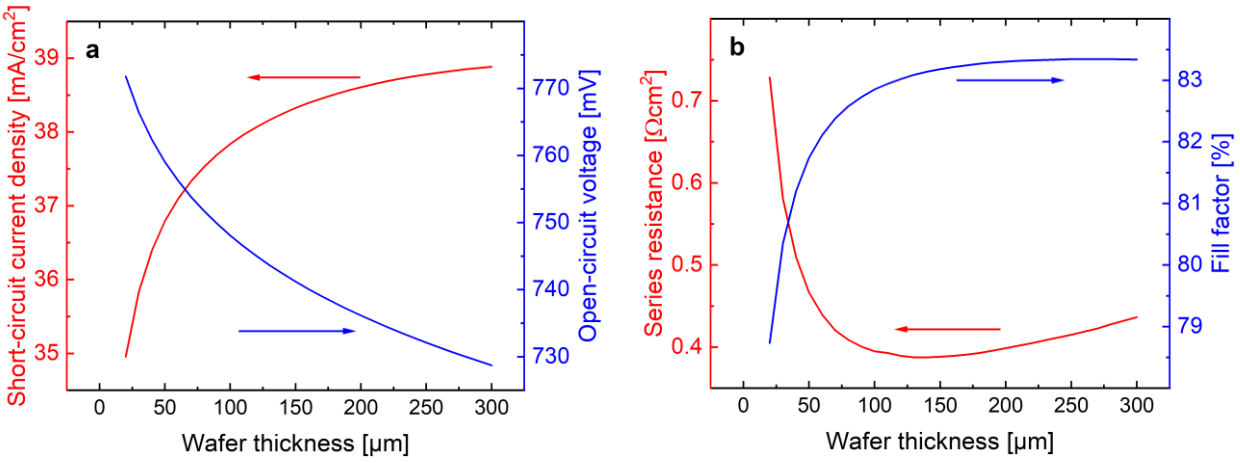

Figure S9 | Simulated solar cell performances of TCO-free SHJ solar cells. a, Short-circuit current density and open-circuit voltage. **b,** Series resistance and fill factor.

The possibility of absorber conducted TCO-free SHJ solar cell with thin Si wafer is simulated in Quokka3. As shown in Fig. S9, the short-circuit current density decreases and the open-circuit

voltage increases when the wafer thickness reduces. The series resistance is lower than 0.6 Ωcm^2 when the wafer thickness is reduced to 30 μm, yielding a fill factor of over 80.3%. This simulation result indicates that the absorber conducted concept can also be used on thin c-Si wafer SHJ solar cells to enable the TCO-free design.

References

1 Couderc, R., Amara, M. & Lemiti, M. Improvement of Back Surface Metallization in a Silicon Interdigitated back Contacts Solar Cell. *Energy Procedia* **38**, 684-690, doi:10.1016/j.egypro.2013.07.333 (2013).

2 Chen, H.-L. *et al.* A 19.9%-efficient ultrathin solar cell based on a 205-nm-thick GaAs absorber and a silver nanostructured back mirror. *Nature Energy* **4**, 761-767, doi:10.1038/s41560-019-0434-y (2019).

3 Holman, Z. C., Descoeudres, A., De Wolf, S. & Ballif, C. Record Infrared Internal Quantum Efficiency in Silicon Heterojunction Solar Cells With Dielectric/Metal Rear Reflectors. *IEEE Journal of Photovoltaics* **3**, 1243-1249, doi:10.1109/jphotov.2013.2276484 (2013).

4 Mette, A. *New Concepts for Front Side Metallization of Industrial Silicon Solar Cells* Doctoral degree thesis, University of Freiburg, (2007).

5 Choi, D., Yoon, H., Kim, K.-H., Um, H.-D. & Seo, K. ITO-free carrier-selective contact for crystalline silicon solar cells. *Journal of Materials Chemistry A* **7**, 2192-2199, doi:10.1039/c8ta11220g (2019).